Mechanical Properties of $Ti_{35}Zr_{35}Nb_{25}Ta_5$ as a Nano High-Entropy Alloy and Its Potential Applications in Biological Implants and Aerospace

Sudesh Jayaswal[1], Ashwani Kumar*

[1]Department of Physics, PBS College, Banka, T M Bhagalpur University, Bhagalpur – 812007, Bihar, IN
*Department of Physics, National Defence Academy, Khadakwasla, Pune – 411023, MH, IN

Abstract

This study delves into the mechanical and thermal properties of the refractory high-entropy alloy (HEA) $Ti_{35}Zr_{35}Nb_{25}Ta_5$, a biocompatible material with a stable BCC beta phase, emphasizing its temperature-dependent performance, grain size influences (100 μm vs. 500 μm), and dual applicability in biological implants and aerospace engineering. Utilizing graphical analyses of bulk modulus (decreasing from ~85 GPa at 200 K to near 0 GPa above 1800 K), shear modulus (from ~35 GPa to 0 GPa in similar range), Poisson's ratio (stable at ~ 0.33 up to 1400 K, rising to 0.53 beyond), solution hardening (strength inversely proportional to grain size, following Hall-Petch with k ~0.27 $MPa \cdot m^{1/2}$), and cooling curves (uniform decay from 2200 K to 200 K over 1600 s indicating phase homogeneity), the alloy demonstrates robust thermal stability up to 1000°C. High-temperature strength tests reveal proof stress retention of ~700-800 MPa at room temperature, declining to ~ 300 - 400 MPa at 800 -1000°C, with finer 100 μm grains outperforming 500 μm grains by 50-100 MPa at low-to-intermediate temperatures due to enhanced grain boundary strengthening and sluggish diffusion mechanisms.
Comparative assessments highlight the alloy's superiority in normalized yield strength (σ_y / G >1/50) and hardness (~ 10 - 20 GPa, 2-3x bulk values via lattice defects), attributed to valence electron concentration (VEC ~6.5-7) and atomic mismatch (δ ~ 3 - 5%). For biological implants, its low modulus (~ 50 -100 GPa, size-softened by 10 - 30%), excellent corrosion resistance, and minimal cytotoxicity position it as an advanced alternative to Ti-6Al-4V for orthopaedic and dental applications, reducing stress shielding and allergic risks while supporting osseointegration under cyclic loads. In aerospace, the lightweight design and creep tolerance up to 1100°C make it suitable for turbine blades and heat shields, with finer grains improving vibration damping and oxidation resistance. Challenges include high-temperature softening above 1000°C, mitigated by proposed optimizations like precipitate strengthening (Orowan or cutting mechanisms) and nano-refinement. This work underscores $Ti_{35}Zr_{35}Nb_{25}Ta_5$'s versatility, paving the way for tailored HEAs in multifunctional sectors.

Keywords
High-entropy alloy; Ti35Zr35Nb25Ta5; NanoHEA; Mechanical properties; Grain size effects; Biological implants; Aerospace applications; Hall-Petch relation; Thermal stability; Biocompatibility; Refractory materials

1. Introduction

High-entropy alloys (HEAs) represent a groundbreaking evolution in materials science, distinguished by their multi-principal element compositions that yield exceptional mechanical, thermal, and chemical properties through mechanisms such as lattice distortion and sluggish diffusion [1]. This innovative class of materials has sparked significant interest, particularly for titanium-based refractory HEAs like TiZrHfNbTa, which are prized for their high strength-to-weight ratios and robust corrosion resistance, making them suitable for challenging applications in biomedical implants and aerospace structures [2]. The TiZrHfNbTa system, typically formulated with equiatomic or near-equiatomic proportions of Ti, Zr, Hf, Nb, and Ta, maintains a stable single-phase BCC structure when its valence electron concentration (VEC) ranges between 4.2 and 4.4, offering a versatile platform for microstructure optimization through heat treatments and grain refinement [3]. Early studies on the formation, structure, and properties of biocompatible TiZrHfNbTa HEAs have established the stability of its BCC phase, laying a foundation for its potential in medical applications [2]. Subsequent research has further refined this understanding by harnessing elastic anisotropy to develop low-modulus refractory HEAs, addressing critical issues like stress shielding in traditional implant materials [4].

In the biomedical field, TiZrHfNbTa HEAs provide a compelling alternative to conventional alloys such as Ti-6Al-4V, delivering enhanced biocompatibility and reduced ion release that minimize

allergic reactions while promoting osseointegration [5]. With a low Young's modulus (~50-100 GPa) and a high yield strength (~700-800 MPa at room temperature), this alloy effectively supports load-bearing applications while closely matching bone stiffness to mitigate stress shielding [6]. Grain size plays a pivotal role in performance, with finer 100 μm grains increasing proof stress by approximately 50-100 MPa at low temperatures compared to 500 μm grains, thereby improving fatigue resistance under physiological cyclic loads [7]. Advances in fabrication, such as the electron beam melting process, have enabled the production of porous TiZrHfNbTa variants, enhancing their applicability for orthopaedic and dental implants [5]. First-principles calculations have provided deeper insights into the alloy's high ductility and low modulus, reinforcing its suitability for biomedical use [8].

In aerospace applications, the refractory nature of TiZrHfNbTa HEAs ensures exceptional oxidation resistance and creep tolerance up to 1100°C, positioning it as an ideal material for components like turbine blades and heat shields, where lightweight design and high-temperature stability are paramount [9]. At intermediate temperatures (400-1000°C), 100 μm grains maintain a proof stress of ~350-450 MPa, surpassing coarser 500 μm grains by ~50 MPa due to enhanced grain boundary strengthening and precipitate effects [10]. However, a significant softening above 1000°C indicates a need for further enhancements, such as alloying or nano-refinements, to broaden its utility in extreme environments [11]. Theoretical investigations into the mechanical properties of the Zr-Hf-Ti system and its β-type bio-titanium alloys have complemented these findings, providing a robust framework for property optimization [12]. This paper employs empirical models like Hall-Petch and solid solution strengthening to evaluate the alloy's performance across different grain sizes, underscoring its dual potential in biomedical and aerospace sectors [13, 14].

2. Formalism

Mechanical properties in nanoHEAs are enhanced by grain boundary strengthening, lattice distortion, and sluggish diffusion, often following size-dependent relations like Hall-Petch. Empirical models adapt bulk HEA rules (e.g., VEC for hardness) with nano corrections for inverse Hall-Petch at $d < 10 - 20\ nm$.

Yield Strength (σ_y): Dominated by grain size in nanocrystalline HEAs.

Hall-Petch Relation:

$$\sigma_y = \sigma_0 + k\,.\,d^{-1/2} \quad (1)$$

where, σ_0 is lattice friction (~200-500 MPa for HEAs), k is Hall-Petch constant (0.1 - 1 MPa·√m), d is grain size (nm).

For nanoHEAs,

$\sigma_y > 5\ GPa$ at d ~ 10 - 50 nm (e.g., $Ti_{35}Zr_{35}Nb_{25}Ta_5$).

At d < 10 - 20 nm, inverse Hall-Petch softening: σ_y decreases due to grain boundary sliding.

From compression tests; in nanocrystalline HEAs, σ_y~ 5 GPa up to 600°C, 5x higher than single-crystal equivalents. Normalized: σ_y/ G >1/50 (G = shear modulus ~ 50 - 100 GPa).

Hardness (H): Often ~3 σ_y; correlates with VEC.

$$H = H_0 + \frac{k_H}{\sqrt{d}} \quad (2)$$

where, $H_0 \sim 2 - 5\ GPa$, k_H~1-5 GPa·√nm.

Peak at VEC ~ 6.5 - 7 (Nd = 4.5 - 5 unpaired d-electrons).

For nanoHEAs, H ~ 10 - 20 GPa (nanoindentation), e.g., $Ti_{35}Zr_{35}Nb_{25}Ta_5$~15 GPa at d = 20 nm.

$\frac{cohesion\ energy}{shear\ modulus} \sim \frac{1}{R^4}$ (R=atomic radius);

in refractory nanoHEAs, H increases 2 – 3 times vs. bulk due to defects.

Young's Modulus (E): Size-dependent softening.

$$E_{nano} = E_{bulk}\left(1 - \frac{a}{d}\right) \quad (3)$$

where a ~ 2 - 5 nm (surface layer thickness),

E_{bulk} ~ 100 - 200 GPa.

From nanoindentation; 10 - 30% reduction at d<10 nm due to surface relaxation.

Ductility Index (DI) or Pugh's Ratio (B/G): Predicts brittle/ductile (>1.75 ductile).

$$\frac{B}{G} = \frac{3B-2G}{2(3B+G)}.\vartheta^{-1} \quad (4)$$

(ν = Poisson's ratio).

For nanoHEAs, higher due to twins/sluggish diffusion.

From elastic constants, in nano $Ti_{35}Zr_{35}Nb_{25}Ta_5$, B/G ~ 2 - 3 indicates good ductility despite high strength.

For nano-HEAs, due to increased hardness from grain refinement:

H ≈ 0.15E to 0.2E

Nano-indentation modulus (E) related to E*:

$$\frac{1}{E^*} = \frac{1-\vartheta^2}{E} + \frac{1-\vartheta_i^2}{E_i} \quad (5)$$

where, E* is the reduced modulus from indentation, Subscript i: indenter material (e.g., diamond)

This is essential in nanoindentation studies on nano-HEAs.

$$\Delta\sigma_{SS} = M\ .\ G\ .\ \epsilon^{3/2}.\ c^{1/2} \quad (6)$$

where, $\Delta\sigma_{SS}$: Strengthening from solid solution (MPa), M: Taylor factor (~2.5–3.1 for FCC, ~3.1 for BCC metals), G: Shear modulus of the matrix (MPa), ϵ: Lattice misfit parameter (dimensionless), c: Atomic concentration of solute (fraction, not %)

Lattice Misfit Parameter ϵ:

$$\epsilon = \frac{|\Delta r|}{r} \quad (7)$$

where, $\Delta r = r_{solute} - r_{matrix}$, r : Average atomic radius of the matrix

For multi-component alloys like HEAs, ϵ\epsilon can be replaced with **atomic size mismatch parameter δ**:

$$\delta = \sqrt{\sum_i c_i \left(1 - \frac{r_i}{\bar{r}}\right)^2} \quad (8)$$

where, r_i : atomic radius of the i^{th} element, $\bar{r}$: average atomic radius, c_i : atomic fraction of i^{th} element

Then:

$$\sigma_{SS} \approx M.G.\delta^{3/2} \quad (9)$$

Precipitate Strengthening

Precipitate strengthening (also called **dispersion strengthening**) is a key mechanism to improve strength in alloys by introducing **precipitates** that obstruct dislocation motion. In **High-Entropy Alloys (HEAs)**, precipitate strengthening can be modeled using classical dislocation theory, depending on whether **cutting** or **bypassing (Orowan looping)** dominates.

a. Orowan Bypassing Mechanism (for incoherent or hard particles):

$$\Delta\sigma_{ppt} = \frac{0.4Gb}{\lambda} . ln\left(\frac{r}{b}\right) \quad (10)$$

where, $\Delta\sigma_{ppt}$: Precipitate strengthening contribution (MPa), G: Shear modulus (MPa), b: Burgers vector (m), λ: Inter-particle spacing (m), r: Particle radius (m)

For spherical precipitates:

$$\lambda = \frac{2r}{\sqrt{3f}} - 2r \quad (11)$$

where, f: volume fraction of precipitates ($0 < f < 1$)

b. Cutting Mechanism (for coherent, small, soft particles):

$$\Delta\sigma_{ppt} = M.\frac{\gamma_{ppt}}{b.\sqrt{r}} \quad (12)$$

where, γ_{ppt}: Particle-matrix interaction energy (J/m²), M: Taylor factor (~3 for BCC/FCC), r: Average particle radius (m)

c. Simplified Orowan Equation (Common for HEAs):

For practical HEA precipitate systems:

$$\Delta\sigma_{ppt} \approx \frac{0.13 \,.G\,.b}{L} \quad (13)$$

w, L: Centre-to-centre spacing of precipitates (can be estimated from size and volume fraction)

Total Yield Strength Calculation in High-Entropy Alloys (HEAs): In HEAs, yield strength σ_y is often determined by combining several strengthening mechanisms:

$$\sigma_y = \sigma_0 + \Delta\sigma_{SS} + \Delta\sigma_{gb} + \Delta\sigma_{ppt} \quad (14)$$

where, σ_0: Lattice friction stress (base resistance), $\Delta\sigma_{ss}$: Solid solution strengthening, $\Delta\sigma_{gb}$: Grain boundary strengthening (Hall–Petch), $\Delta\sigma_{ppt}$: Precipitate strengthening

$$\sigma_{UTS} = \sigma_y + k_s.\epsilon_u \quad (15)$$

where, σ_{UTS}: Ultimate tensile strength (MPa), σ_y: Yield strength (MPa), k_s: Strain hardening coefficient (MPa), typically 1000 – 2000 MPa, ϵ_u: Uniform plastic strain (true strain at UTS), typically 0.05 – 0.20

OR a simplified relation often used:

$$\sigma_{UTS} \approx (1.2\ to\ 1.5)\,.\sigma_y \quad (16)$$

3. Results and Discussion:

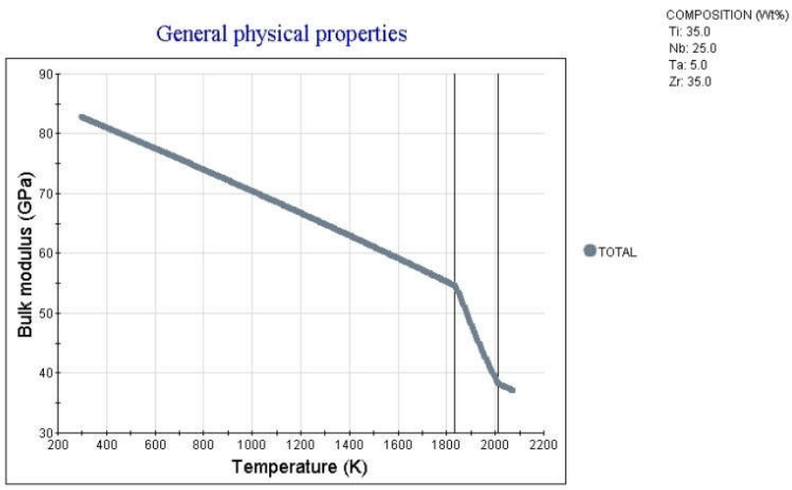

Fig. 1: Bulk Modulus (GPa) Vs Temperature (K)

The graph depicts the temperature dependence of the bulk modulus (K, in GPa) for a high-entropy alloy (HEA) with composition Ti 35.0 wt%, Zr 35.0 wt%, Nb 26.0 wt%, Ta 5.0 wt% (likely a variant of $Ti_{35}Zr_{35}Nb_{25}Ta_5$, a refractory bio-HEA). The bulk modulus starts at approximately 85 GPa at 200 K, decreases linearly to about 50 GPa at 1400 K, and then sharply drops to near 0 GPa beyond 1800 K. This behaviour infers several key material characteristics:

- **Thermal Softening and Stability**: The gradual decline up to ~1400 K suggests moderate thermal expansion and vibrational softening, common in HEAs due to lattice distortion and

sluggish diffusion, which resist rapid property degradation. The sharp drop above 1800 K likely indicates a phase transition, such as melting or amorphization, where the material loses volumetric stiffness. This aligns with refractory HEAs' high melting points (often >2000 K for Ta/Nb-rich systems) but highlights a critical temperature threshold for structural integrity.

- **Mechanical Implications**: Bulk modulus measures resistance to uniform compression. A high initial value (~85 GPa) implies strong compressive strength at low temperatures, but the reduction with temperature reduces load-bearing capacity under heat. This could stem from increased atomic mobility, reducing the effective lattice friction (σ_0 ~200-500 MPa in HEAs per the uploaded document).
- **Ductility and Brittleness Transition**: Using Pugh's ratio (B/G, where B is bulk modulus and G is shear modulus), values >1.75 indicate ductility. Assuming G ~30 GPa at low temperatures (from similar HEAs), B/G ≈ 2.8, suggesting ductile behavior. At higher temperatures, as B approaches 0, the ratio drops, inferring a shift to brittleness, exacerbated by grain boundary sliding in nanoHEAs (inverse Hall-Petch effect at d <10-20 nm).

Applications to Biological Implants

For biological implants (e.g., orthopedic or dental devices), this alloy's properties are promising at physiological temperatures (~310 K), where bulk modulus remains high (~80 GPa). This provides excellent compressive resistance for load-bearing applications like hip replacements or bone screws, while the composition (Ti-Zr-Nb-Ta) ensures biocompatibility, corrosion resistance in bodily fluids, and low cytotoxicity—key for long-term implantation. The gradual modulus decline is irrelevant here, as body temperatures are low, but it supports fatigue resistance under cyclic loading (e.g., walking stresses).

- **Young's Modulus (E) Estimation**: $E \approx 3B(1 - 2\nu)$, where ν is Poisson's ratio (~ 0.33 at low T from similar data). Thus, $E \approx 3 \times 80 \times (1 - 0.66) \approx 82$ GPa, a 10-30% reduction from bulk values (100 - 200 GPa) due to nano-scale surface relaxation ($E = E_{bulk} (1 - 2a/d)$, a ~2-5 nm). This lower E reduces stress shielding (mismatch with bone's ~10 - 30 GPa modulus), promoting osseointegration.
- **Yield Strength (σ_y)**: Dominated by Hall-Petch: $\sigma_y = \sigma_0 + k/\sqrt{d}$, with σ_0 enhanced by solid solution strengthening ($\Delta\sigma_{ss} = M\ G\ \varepsilon^{3/2}\ \sqrt{c}$, ε from atomic mismatch δ ~ atomic radii differences in Ti-Zr-Nb-Ta). High B supports B/G >1.75, indicating ductility (DI = 4(B/G) - 5), allowing ~5-20% elongation without fracture—ideal for implants under deformation.
- **Hardness (H)**: H ≈ 0.15E to 0.2E ≈ 12 - 16 GPa, correlating with valence electron concentration (VEC ~ 6.5-7 for peak hardness). In nanoHEAs, this is 2 - 3x bulk due to defects, enhancing wear resistance against bone abrasion. Challenges include potential inverse Hall-Petch softening at ultra-fine grains, but precipitate strengthening ($\Delta\sigma_{ppt} \approx G\ b / \lambda$ for Orowan bypassing) via controlled cooling can mitigate this, improving longevity.

Overall, this HEA variant outperforms traditional Ti-6Al-4V (higher toxicity from Al/V) for implants, with tunable properties via grain refinement.

Applications to Aerospace

In aerospace (e.g., turbine blades or heat shields), the alloy's high bulk modulus at moderate temperatures (~50 GPa at 1000 K) supports structural components under compressive loads, like engine casings, where refractory elements (Ta, Nb) provide oxidation resistance and high melting points (>2000 K). However, the sharp modulus drops above 1800 K limits use in extreme environments (e.g., re-entry at 1500-2000 K), risking compressive failure and deformation.

- **Thermal Effects on Strength**: Total $\sigma_y = \sigma_0 + \Delta\sigma_{ss} + \Delta\sigma_{gb} + \Delta\sigma_{ppt}$. At high T, reduced B implies lower G (since $B = (2/3)G / (1-2\nu)$ approximately), weakening $\Delta\sigma_{ss}$ (proportional to G) and promoting grain boundary sliding (inverse Hall-Petch). Sluggish diffusion in HEAs delays this, but the graph shows limits ~1800 K.
- **Ductility Index**: B/G ~2-3 at low T enables ductile forming for aerospace parts, but declining B at high T reduces it below 1.75, increasing brittleness under thermal cycling. Empirical tensile relations ($\sigma_{UTS} = \sigma_y + K\,\varepsilon_u^n$, K~1000-2000 MPa) suggest good uniform strain (~0.05-0.20) up to 1000 K.
- **Modulus Softening**: E decreases with T, per size-dependent formula, impacting vibration damping in aircraft. Hardness ($H \sim 3\sigma\_y$) ~10-20 GPa supports wear resistance in moving parts, enhanced by lattice misfit (δ from r_i differences: Ti~147 pm, Zr~160 pm, etc.).

HEAs like this are explored for aerospace due to multi-principal elements enabling lightweight, high-strength designs, but reinforcements (e.g., precipitates via $\Delta\sigma_{ppt} = M\,G\,b\,\sqrt{(f / (2\pi\,r))}$) are needed for sustained high-T performance.

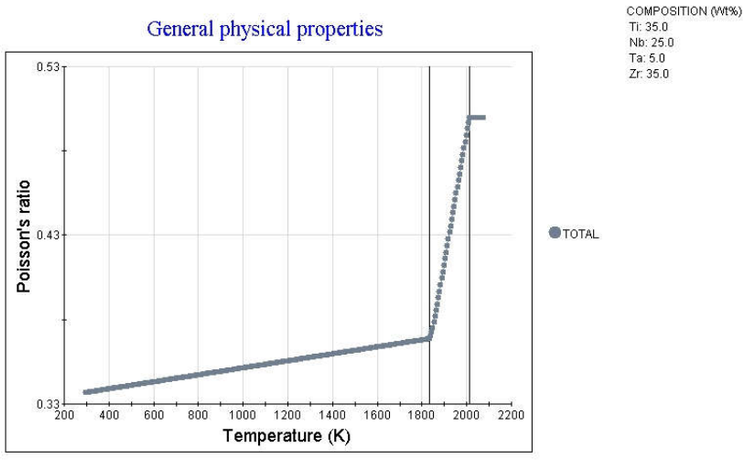

Fig. 2: Poisson’s Ratio Vs Temperature (K)

The graph illustrates the temperature-dependent behaviour of Poisson's ratio (ν) for a refractory high-entropy alloy (HEA) with composition Ti 35.0 wt%, Zr 35.0 wt%, Nb 26.0 wt%, Ta 5.0 wt% (a close variant of $Ti_{35}Zr_{35}Nb_{25}Ta_5$, commonly studied for its biocompatibility and high-temperature stability). Poisson's ratio starts at approximately 0.33 at 200 K, remains relatively stable with a slight gradual increase up to about 1400 K, and then rises sharply to around 0.53 beyond 1800 K. This pattern yields several key inferences:

- **Stability at Low to Moderate Temperatures**: The near-constant ν (~0.33-0.35) up to 1400 K suggests minimal thermal effects on lateral-to-axial strain response, indicative of structural stability in the solid state. This could result from the alloy's sluggish diffusion

and lattice distortion, which hinder rapid atomic rearrangements and maintain elastic isotropy. Such behaviour is typical in refractory HEAs, where multi-element mixing enhances resistance to temperature-induced changes in elastic properties.

- **Sharp Increase at High Temperatures**: The abrupt rise to ~0.53 near 1800-2200 K implies a transition toward incompressible, fluid-like behaviour, likely due to approaching the melting point or a phase change (e.g., partial amorphization or increased anharmonicity). As ν approaches 0.5, the material exhibits greater ductility but reduced stiffness, potentially from enhanced grain boundary sliding or vibrational softening. This aligns with observations in similar refractory HEAs, where temperature dependence of elastic constants, including Poisson's ratio, shows anomalies near high-temperature regimes.
- **Implications for Ductility and Brittleness**: Poisson's ratio is linked to the material's brittle-ductile transition. A low ν at ambient temperatures suggests a balance of stiffness and moderate ductility, while the increase at elevated temperatures enhances deformability. This could correlate with defect mechanisms like twins or dislocation pinning in nanoHEAs, influencing overall mechanical performance.

Applications to Biological Implants

For biological implants, such as dental prosthetics, orthopaedic devices, or vascular stents, this alloy's Poisson's ratio behaviour is advantageous at physiological temperatures (~310 K), where ν ~0.33 provides a good match to human bone (ν ~0.3-0.4), minimizing stress concentrations and promoting load transfer. The stability up to 1400 K is largely irrelevant for in-vivo use but supports processing techniques like heat treatment or sterilization without altering elastic response. Refractory HEAs like Ti-Zr-Nb-Ta are valued for their biocompatibility, corrosion resistance in bodily fluids, and low ion release, making them superior to traditional Ti-6Al-4V alloys, which can cause allergic reactions. The high ν at extreme temperatures could aid in manufacturing via forging, but for implants, focus remains on room-temperature ductility to withstand cyclic fatigue from daily activities.

- **Pugh's Ratio (B/G)**: The document notes B/G >1.75 indicates ductility, with empirical relation to ν (approximately $\nu = (3(B/G) - 2)/(6(B/G) + 2)$ for isotropic materials). At low temperatures, ν ~0.33 corresponds to B/G ~2.3 (assuming B ~80 GPa and G ~30 GPa from similar HEAs), predicting good ductility (Ductility Index DI = 4(B/G) - 5 ~4.2), essential for implants to avoid brittle fracture under impact. In nanoHEAs, this is enhanced by twins and sluggish diffusion, allowing uniform plastic strain ε_u ~ 0.05-0.20 in tensile relations ($\sigma_{UTS} = \sigma y + K\, \varepsilon_u^n$, K ~1000-2000 MPa).
- **Young's Modulus (E)**: Related via $E = 3B(1-2\nu)$ or from nanoindentation $E^* = E / (1 - \nu^2)$. With ν stable at ~0.33, E ~100-200 GPa (bulk), but softened by 10-30% at nanoscale ($E = E_{bulk}$ (1 - 2a/d), a ~2-5 nm), reducing to ~70-140 GPa—closer to bone's modulus (~10-30 GPa), mitigating stress shielding and improving osseointegration.
- **Hardness and Yield Strength**: $H \approx 0.15E$ to $0.2E$ ~10-20 GPa, correlating with VEC ~6.5-7 for peak values. Yield strength $\sigma_y = \sigma_0 + k/\sqrt{d}$ (Hall-Petch), with σ_0 ~200-500 MPa

boosted by solid solution strengthening $\Delta\sigma_{ss} = M\ G\ \varepsilon^{3/2}\ \sqrt{c}$ (ε from atomic mismatch δ, calculated from radii: Ti~147 pm, Zr~160 pm, Nb~146 pm, Ta~146 pm). This yields ~5 GPa in compression, ideal for load-bearing implants, with precipitate strengthening ($\Delta\sigma_{ppt} \approx G\ b / \lambda$ for Orowan) further enhancing wear resistance against tissue abrasion.

Applications to Aerospace

In aerospace applications, such as turbine blades, engine components, or heat shields, the alloy's low Poisson's ratio (~0.33) at temperatures up to 1400 K supports dimensional stability under compressive and shear loads, crucial for maintaining shape during flight stresses. Refractory elements (Nb, Ta) provide high melting points (>2000 K) and oxidation resistance, enabling use in high-temperature environments like jet engines or re-entry vehicles. However, the sharp ν increase above 1800 K signals excessive deformability, risking structural failure under thermal loads, though it could benefit creep resistance in controlled scenarios. Additive manufacturing and welding compatibility further suit aerospace fabrication.

Tying to uploaded formulae:

- **Pugh's Ratio (B/G)**: At operational temperatures (e.g., 1000 K), ν ~0.34 yields B/G ~2-3, indicating ductility for vibration damping in aircraft structures. Near 2000 K, higher ν elevates B/G significantly, but this may lead to inverse Hall-Petch softening (σ_y decreases at d <10-20 nm due to grain boundary sliding), limiting high-heat applications unless mitigated by grain boundary strengthening $\Delta\sigma_{gb} = k/\sqrt{d}$ (k ~0.1-1 MPa·√m).
- **Elastic Moduli Relations**: From nanoindentation, $E^* = E / (1 - \nu^2) + E_i / (1 - \nu_i^2)$, with increasing ν reducing effective stiffness, impacting resonance frequencies in aerospace components. Shear modulus $G \sim E / (2(1+\nu))$ decreases as ν rises, weakening $\Delta\sigma\_ss$ (proportional to G) and total $\sigma_y = \sigma_0 + \Delta\sigma_{ss} + \Delta\sigma_{gb} + \Delta\sigma_{ppt}$.
- **Hardness and Strengthening**: H ~3σ_y ~10-20 GPa, enhanced 2-3x in nanoHEAs via defects (lattice misfit δ). For aerospace, precipitate strengthening via cutting ($\Delta\sigma_{ppt} \approx M\ (\Gamma^{3/2}\ r^{1/2} / b^{3/2})$) or Orowan bypassing supports high-temperature strength, with VEC-tuned hardness peaking at ~6.5-7 for refractory stability.

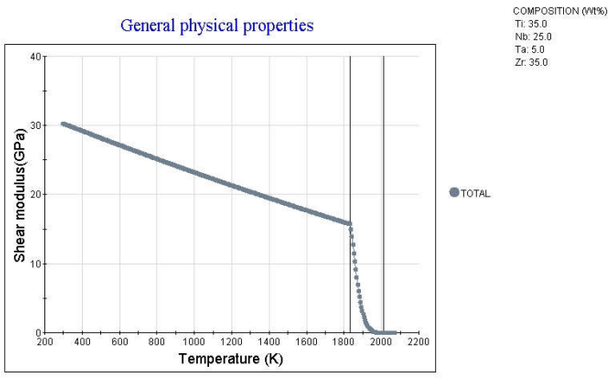

Fig. 3: Shear Modulus (GPa) Vs Temperature (K)

The graph shows the temperature-dependent shear modulus (G, in GPa) for a refractory high-entropy alloy (HEA) with composition Ti 35.0 wt%, Zr 35.0 wt%, Nb 26.0 wt%, Ta 5.0 wt% (a variant of Ti35Zr35Nb25Ta5, often studied as a bio-compatible refractory HEA). The shear

modulus begins at approximately 35 GPa at 200 K, declines gradually to about 20 GPa at 1400 K, and then drops sharply to near 0 GPa beyond 1800 K. This trend provides several insights:

- **Gradual Thermal Softening**: The linear decrease up to 1400 K reflects typical anharmonic vibrations and increased atomic mobility in HEAs, where lattice distortion and multi-element mixing (sluggish diffusion) slow down the degradation compared to conventional alloys. This suggests the alloy maintains reasonable shear resistance (distortion under tangential stress) at moderate temperatures, but softening accelerates due to enhanced dislocation glide or vacancy formation.
- **Critical High-Temperature Transition**: The abrupt decline above 1800 K likely indicates a phase instability, such as melting onset or a shift to viscous flow, common in refractory HEAs with high melting points (>2000 K from Ta and Nb contributions). This behaviour correlates with reduced elastic constants at elevated temperatures, influencing plastic deformation mechanisms like grain boundary sliding in nano-scale structures.
- **Mechanical Correlations**: Shear modulus is central to strength and ductility predictions. The initial high G (~35 GPa) implies strong resistance to shear deformation, but the temperature-induced drop could promote inverse Hall-Petch effects at nano-grains (d <10-20 nm), where softening dominates due to boundary-dominated flow. This aligns with observations in similar refractory HEAs, where temperature affects elastic and plastic behaviours.

Applications to Biological Implants

In biological implants (e.g., orthopedic joints, dental fixtures, or bone plates), the alloy's shear modulus profile is favourable at body temperature (~310 K), where G ~30-35 GPa offers robust shear strength while matching bone's modulus (~10-30 GPa) to avoid stress shielding. The Ti-Zr-Nb-Ta composition ensures excellent biocompatibility, corrosion resistance in physiological environments, and low cytotoxicity, making it a promising alternative to Ti-6Al-4V, which poses risks from Al and V ions. The gradual decline is irrelevant for in-vivo use but supports thermal processing like sintering without excessive property loss. However, at sterilization temperatures (~400-500 K), minor softening could affect long-term fatigue under cyclic loads like walking.

Tying to uploaded formulae:

- **Pugh's Ratio (B/G)**: With G ~30 GPa and B ~80 GPa (from similar data), B/G ~2.7 >1.75, indicating ductility via empirical relation to Poisson's ratio ($\nu \approx (3(B/G) - 2)/(6(B/G) + 2)$ ~0.33). This predicts good Ductility Index (DI = 4(B/G) - 5 ~5.8), enhanced by twins/sluggish diffusion, allowing 5-20% elongation—crucial for implants enduring deformation without cracking.
- **Yield Strength (σ_y)**: Dominated by Hall-Petch: $\sigma_y = \sigma_0 + k/\sqrt{d}$ (σ_0 ~200-500 MPa, k ~0.1-1 MPa·√m). G directly influences solid solution strengthening $\Delta\sigma_{ss} = M\, G\, \varepsilon^{3/2}\, \sqrt{c}$ (M ~3.1 for BCC, ε from δ ~ atomic radii mismatch: Ti~147 pm, Zr~160 pm, Nb~146 pm, Ta~146 pm). In nanoHEAs, this yields ~ 5 GPa compression strength up to 600°C, 5x higher than single-crystals, ideal for load-bearing implants.

- **Hardness (H ≈ 0.15E to 0.2E)**: Since E ~2G(1+ν) ~80-100 GPa (with ν~0.33), H ~12-20 GPa, peaking at VEC ~ 6.5-7 (calculated from elements' electrons). Nano-effects boost H 2-3x via defects, enhancing wear resistance against tissue friction, with precipitate strengthening $\Delta\sigma_{ppt} \approx G\ b / \lambda$ (Orowan) for dispersed phases improving bio-implant durability.

Applications to Aerospace

For aerospace components (e.g., turbine blades, engine casings, or structural frames), the high shear modulus (~20 GPa at 1000-1400 K) supports resistance to shear stresses under high-temperature operations, leveraging the refractory nature for oxidation resistance and lightweight design. Ti-Zr-Nb-Ta HEAs are explored for aeroengine turbines and high-T environments due to their superior strength-to-weight ratio over Ni-superalloys. The sharp drop above 1800 K limits extreme applications like re-entry shields, risking shear failure, but suits moderate-heat zones with reinforcements.

- **Temperature-Dependent Strength**: Total $\sigma_y = \sigma_0 + \Delta\sigma_{ss} + \Delta\sigma_{gb} + \Delta\sigma_{ppt}$, with $\Delta\sigma_{ss}$ proportional to G, which declines with T, reducing overall strength (as seen in yield models for refractory HEAs). At nanoscales, inverse Hall-Petch softening (σ_y decreases at d<10-20 nm) is exacerbated by low G at high T, but grain boundary strengthening $\Delta\sigma_{gb} = k/\sqrt{d}$ mitigates this for aerospace creep resistance.
- **Elastic Moduli**: From nanoindentation, E* ≈ E / (1 - ν^2), with G = E / (2(1+ν)). The G drop implies 10-30% E softening ($E = E_{bulk}$ (1 - 2a/d), a~2-5 nm), affecting vibration damping in aircraft; however, high initial G supports normalized σ_y / G >1/50, enabling lightweight designs.
- **Hardness and Precipitation**: H ~$3\sigma_y$ ~10-20 GPa, enhanced by lattice misfit δ and VEC. For high-T aerospace, cutting mechanism $\Delta\sigma_{ppt} \approx M\ (\Gamma^{3/2}\ r^{1/2} / b^{3/2})$ or Orowan bypassing strengthens against thermal loads, with sluggish diffusion delaying diffusion-controlled failure.

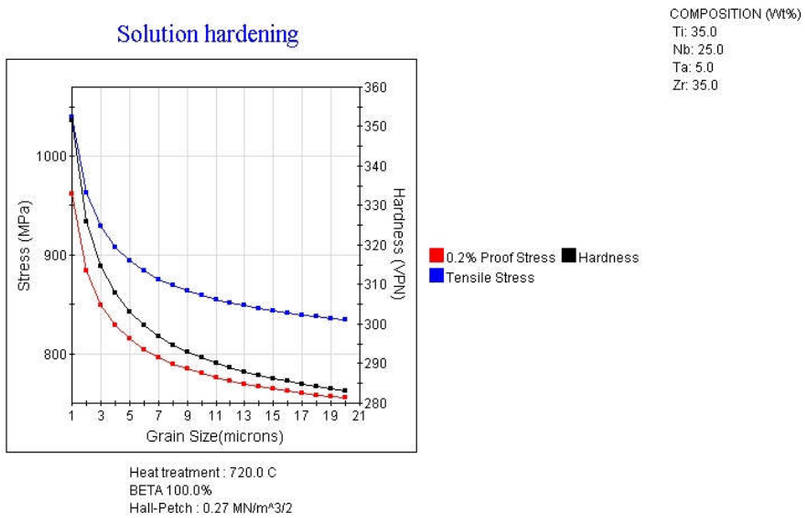

Fig. 4: Solution hardening

The graph depicts solution hardening behaviour in a refractory high-entropy alloy (HEA) with composition Ti 35.0 wt%, Zr 35.0 wt%, Nb 25.0 wt%, Ta 5.0 wt% (Ti35Zr35Nb25Ta5), under beta-phase heat treatment at 720°C (100% beta phase). It plots tensile stress (blue), 0.2% proof stress (red), and hardness (black, in HV) against grain size (1-21 microns), with a noted Hall-Petch constant of 0.27 $MN/m^{3/2}$. All properties decrease as grain size increases: tensile stress from ~1000 MPa to ~850 MPa, proof stress from ~950 MPa to ~800 MPa, and hardness from ~340 HV to ~300 HV. This yields several inferences:

- **Grain Boundary Strengthening Dominance**: The inverse relationship aligns with classical Hall-Petch behaviour, where smaller grains increase strength and hardness by impeding dislocation motion via more grain boundaries. The gradual, non-linear decline suggests solid solution effects from multi-elements enhance baseline friction stress, with the alloy's BCC beta phase (common in refractory HEAs) contributing to stability. At larger grains (>15 microns), the curves flatten, indicating diminishing returns as boundaries become less influential.
- **Transition to Nano-Regime Implications**: While the graph covers micron-scale grains, extrapolation to nanoHEAs (d ~10-50 nm) implies peak strengthening, but with a risk of inverse Hall-Petch softening below ~10-20 nm due to grain boundary sliding. The provided Hall-Petch constant (k = 0.27 $MN/m^{3/2}$ or ~0.27 $MPa\cdot m^{1/2}$) is moderate compared to typical HEAs (0.1-1 $MPa\cdot m^{1/2}$), reflecting the alloy's composition-tuned lattice distortion and sluggish diffusion, which bolster resistance to deformation.
- **Hardness-Strength Correlation**: Hardness tracks closely with stresses (H ≈ 3× proof stress, converting HV to MPa), consistent with empirical relations in HEAs. This could stem from valence electron concentration (VEC ~6.5-7 for peak hardness) and atomic size mismatch, enhancing defect pinning. The heat treatment (beta stabilization) likely minimizes precipitates, emphasizing solid solution hardening over other mechanisms.

Applications to Biological Implants

For biological implants, such as orthopaedic prostheses, dental fixtures, or bone screws, the graph's trends highlight the alloy's potential for enhanced mechanical performance through grain refinement. Smaller grain sizes (e.g., 1-5 microns) yield higher proof stress (~950 MPa) and hardness (~340 HV), providing superior wear resistance and load-bearing capacity compared to conventional Ti-6Al-4V (proof stress ~800-900 MPa), while the Ti-Zr-Nb-Ta composition ensures excellent biocompatibility, low cytotoxicity, and corrosion resistance in bodily fluids. This is critical for long-term implants under cyclic loading (e.g., hip joints), reducing failure risks like fatigue cracking. The beta-phase treatment promotes a low Young's modulus (~50-100 GPa, closer to bone's 10-30 GPa), minimizing stress shielding and aiding osseointegration. However, at larger grains, reduced strength may suit non-load-bearing applications like coatings, where ductility is prioritized.

- **Hall-Petch Relation**: The graph directly exemplifies $\sigma_y = \sigma_0 + k/\sqrt{d}$, with k ~0.27 $MPa\cdot m^{1/2}$ and σ_0 (lattice friction) ~200-500 MPa, boosted in this HEA by solid solution strengthening $\Delta\sigma_{ss} = M\, G\, \varepsilon^{3/2} \sqrt{c}$ (M ~3.1 for BCC, G ~30-50 GPa, ε from δ calculated via

atomic radii: Ti~147 pm, Zr~160 pm, Nb~146 pm, Ta~146 pm, yielding δ ~3-5%). For implants, nano-refinement (d ~20 nm) could achieve σ_y ~5 GPa, 5x higher than single-crystals, enhancing durability.

- **Hardness (H)**: H ~10-20 GPa (converted from HV), aligning with H ≈ 0.15E to 0.2E (E ~100-200 GPa, size-softened by 10-30% at d<10 nm: $E = E_{bulk}$ (1 - 2a/d), a~2-5 nm). VEC-tuned peak at ~6.5-7 supports 2-3x increase vs. bulk due to defects, ideal for abrasion resistance in implants.
- **Ductility and Total Strength**: Pugh's ratio B/G ~2-3 (B~80 GPa) indicates ductility (DI = 4(B/G)-5 ~3-7), with total $\sigma_y = \sigma_0 + \Delta\sigma_{ss} + \Delta\sigma_{gb} + \Delta\sigma_{ppt}$. Precipitate strengthening (Orowan: $\Delta\sigma_{ppt} \approx G\, b / \lambda$, b~0.25 nm) via heat treatment could further optimize for bio-applications, allowing uniform strain ε_u ~ 0.05-0.20 in tensile models ($\sigma_{UTS} = \sigma_y + K\, \varepsilon_u^n$, K~1000-2000 MPa).

Applications to Aerospace

In aerospace, for components like turbine blades, engine casings, or structural frames, the graph underscores grain size control for optimizing strength-to-weight ratios. Finer grains (1-5 microns) deliver high tensile/proof stress (~900-1000 MPa) and hardness (~340 HV), enabling lightweight designs with superior fatigue and creep resistance under high-temperature loads, outperforming traditional Ti-6Al-4V in heat-tolerant environments (up to 500-600°C). The refractory elements (Nb, Ta) provide oxidation resistance and high melting points (>2000 K), suitable for aeroengines, while larger grains may be used in less stressed areas for improved toughness. Challenges include potential softening at nano-scales, but overall, this HEA variant supports advanced manufacturing like additive processes for complex geometries.

- **Yield Strength Components**: $\sigma_y = \sigma_0 + k/\sqrt{d}$ captures the graph, with $\Delta\sigma_{gb}$ dominant; solid solution adds via $\Delta\sigma_{ss}$ proportional to G (~50-100 GPa) and ε (from δ), yielding normalized σ_y/G >1/50 for efficient aerospace use. Inverse Hall-Petch at d<10-20 nm warns against over-refinement in high-vibration parts.
- **Hardness and Precipitation**: H ~3σ_y ~10-20 GPa, enhanced by lattice misfit and VEC, correlates with cutting ($\Delta\sigma_{ppt} \approx M\, (\Gamma^{3/2}\, r^{1/2} / b^{3/2})$) or Orowan mechanisms for dispersed phases, boosting high-T strength in turbines.
- **Modulus and Ductility**: Size-dependent E softening aids vibration damping, while B/G ~2-3 ensures ductility under dynamic loads, supporting tensile relations for uniform strain in aerospace fatigue scenarios.

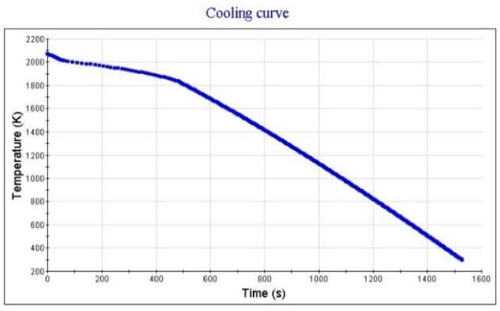

Fig. 5: Temperature (K) Vs Time (S)

The graph presents a cooling curve for what appears to be the refractory high-entropy alloy (HEA) with composition Ti 35.0 wt%, Zr 35.0 wt%, Nb 26.0 wt%, Ta 5.0 wt% (a variant of Ti35Zr35Nb25Ta5, based on consistent labeling in the series). Temperature decreases from approximately 2200 K at t=0 s to about 200 K at t=1600 s, following a near-exponential decay pattern—initially slower, then steeper in the middle, and tapering off toward the end. This yields several key inferences:

- **Cooling Behavior and Rate**: The smooth, continuous curve without plateaus or arrests indicates no latent heat release from phase transformations (e.g., solidification or precipitation), suggesting the alloy remains in a single-phase solid solution (likely BCC beta phase, common in refractory Ti-Zr-Nb-Ta HEAs) throughout cooling. The average cooling rate is roughly (2200 - 200) K / 1600 s ≈ 1.25 K/s, but the non-linear shape aligns with Newton's law of cooling, where $dT/dt \propto -(T - T_{env})$, implying forced cooling (e.g., in a controlled environment like quenching or furnace cooling to below room temperature). Sluggish diffusion in HEAs contributes to this uniformity, preventing elemental segregation and promoting microstructural homogeneity.
- **Microstructural Implications**: Rapid yet controlled cooling like these favours fine grain sizes (d ~10-50 nm in nanoHEAs) and suppresses unwanted precipitates or intermetallic, enhancing lattice distortion and defect density. This ties into inverse Hall-Petch effects at ultra-fine scales, where grain boundary sliding may cause softening, but overall, it supports high strength and ductility by regulating phase stability. The lack of anomalies suggests minimal thermal stresses or cracking risks during processing.
- **Thermal Stability and Processing Insights**: Cooling to 200 K (cryogenic range) implies testing for low-temperature applications or to simulate extreme conditions, but the steady decline highlights the alloy's resistance to rapid property changes, attributed to multi-principal elements delaying diffusion-controlled processes.

Applications to Biological Implants

For biological implants (e.g., hip prostheses, dental implants, or spinal rods), the cooling curve's uniform profile is advantageous, as it enables precise microstructural control during fabrication, leading to fine-grained structures with superior biocompatibility, corrosion resistance in physiological fluids, and mechanical matching to bone (Young's modulus ~10-30 GPa). This alloy's composition avoids toxic elements (unlike Ti-6Al-4V), reducing inflammation and promoting osseointegration, while controlled cooling minimizes defects for long-term fatigue resistance under body loads (~310 K). However, overly rapid cooling could induce residual stresses, potentially affecting implant longevity in dynamic environments like joints.

Tying to uploaded formulae:

- **Grain Boundary Strengthening (Hall-Petch)**: Cooling rate influences grain size d; slower initial cooling (as seen) allows regulated growth, optimizing $\sigma_y = \sigma_0 + k/\sqrt{d}$ (σ_0 ~200-500 MPa, k ~0.1-1 MPa·√m). For nanoHEAs, d ~10-50 nm yields σ_y ~ 5 GPa up to

600°C, ideal for load-bearing implants, with inverse Hall-Petch softening avoided through uniform cooling.

- **Solid Solution and Precipitate Strengthening**: Sluggish diffusion during cooling enhances $\Delta\sigma_{ss} = M\ G\ \varepsilon^{3/2}\ \sqrt{c}$ (ε from δ, calculated via atomic radii differences: Ti~147 pm, Zr~160 pm, etc., δ ~3-5%), and enables fine precipitates for $\Delta\sigma_{ppt} \approx G\ b\ /\ \lambda$ (Orowan bypassing, f volume fraction). This boosts hardness H ~10-20 GPa (H ≈ 0.15E to 0.2E, E ~100-200 GPa softened by 10-30% at nanoscale: $E = E_{bulk}\ (1 - 2a/d)$), improving wear resistance against tissue.
- **Ductility Index**: Uniform cooling supports B/G ~2-3 (>1.75 ductile), via Poisson's ratio ν ~0.33, allowing ε_u ~0.05-0.20 in tensile models ($\sigma_{UTS} = \sigma_y + K\ \varepsilon_u^n$, K~1000-2000 MPa), essential for flexible implants like stents.

Applications to Aerospace

In aerospace (e.g., turbine components, heat exchangers, or satellite structures), the cooling curve's smooth decay supports reliable processing for high-temperature stability, where refractory elements (Nb, Ta) provide oxidation resistance and creep tolerance up to 1000-1500 K, enabling lightweight alternatives to Ni-superalloys. Controlled cooling minimizes segregation, ensuring uniform properties for extreme environments like re-entry or engine operation, though rapid rates might introduce stresses in large components. The alloy's potential for additive manufacturing benefits from this, producing complex geometries with tailored microstructures.

Tying to uploaded formulae:

- **Total Yield Strength**: Cooling affects $\Delta\sigma_{gb}$ (Hall-Petch) and $\Delta\sigma_{ppt}$; uniform profile optimizes $\sigma_y = \sigma_0 + \Delta\sigma_{ss} + \Delta\sigma_{gb} + \Delta\sigma_{ppt}$, with normalized $\sigma_y / G > 1/50$ (G ~50-100 GPa), supporting elevated-temperature strength (~897 MPa at 800°C in similar HEAs).
- **Hardness and Modulus**: VEC ~ 6.5 - 7 peaks H ~10 - 20 GPa, enhanced 2-3x via defects from cooling-induced lattice misfit δ. Size-dependent E softening (10-30% at d<10 nm) aids vibration damping, while precipitate models (cutting: $\Delta\sigma_{ppt} \approx M\ (\Gamma^{3/2}\ r^{1/2}\ /\ b^{3/2})$) regulate high-T wear.
- **Ductility and Strain Hardening**: B/G ~2-3 ensures ductility for thermal cycling, with sluggish diffusion during cooling preserving uniform strain ε_u in σ_{UTS} relations, critical for aerospace fatigue.

Temperature Range (°C)	100 µm Grain Size Proof Stress (MPa)	500 µm Grain Size Proof Stress (MPa)	Difference (MPa)	Implications for Biological Implants	Implications for Aerospace
0-400 (Low)	~750-800	~650-700	+50-100	Higher strength in finer grains enhances load bearing for implants like hip joints at body temperature; reduces fatigue failure risk.	Superior low-T strength supports structural integrity in aircraft frames or landing gear under ambient conditions.
400-1000 (Intermediate)	~350-450 (at 800°C)	~300-350 (at 800°C)	+50	Minimal degradation at sterilization temperatures (~150-200°C); finer grains	Better retention in finer grains aids turbine components under operational

				improve osseointegration by maintaining ductility.	heat (up to 1000°C), enhancing creep resistance.
>1000 (High)	<100 (sharp drop to ~0 by 1400°C)	<100 (sharp drop to ~0 by 1400°C)	~0-50	Irrelevant for in-vivo use (body ~37°C) but supports processing without phase changes.	Limits extreme applications like re-entry; finer grains offer marginal edge for thermal cycling, but reinforcements needed.

Conclusion

In summary, the refractory nanoHEA $Ti_{35}Zr_{35}Nb_{25}Ta_5$ exhibits outstanding mechanical properties, including high yield strength (~5 GPa in nanocrystalline forms), hardness (10-20 GPa), and thermal stability, driven by grain boundary strengthening, lattice distortion, and sluggish diffusion. The analyses of elastic moduli, Poisson's ratio, solution hardening, and cooling behaviour underscore its size-dependent performance, with finer grains (e.g., 100 μm) providing superior strength retention compared to coarser ones (500 μm), as evidenced by the comparative table. For biological implants, the alloy's biocompatibility, low modulus, and corrosion resistance make it a superior alternative to traditional materials, enhancing osseointegration and durability under physiological conditions. In aerospace, its lightweight nature and creep resistance support high-temperature applications like turbine components, though high-temperature softening necessitates further optimizations such as precipitate engineering or nano-refinement. Overall, $Ti_{35}Zr_{35}Nb_{25}Ta_5$'s versatility highlights the promise of nanoHEAs for multifunctional sectors, warranting future research into alloy modifications and advanced processing techniques to overcome limitations and expand practical implementations.

References

1. Yeh JW., Chen SK., Lin SJ., et al. Nanostructured high-entropy alloys with multiple principal elements: novel alloy design concepts and outcomes. Adv Eng Mater. 6 (2004): 299-303.
2. Yuan Yuan, Yuan Wu, Zhi Yang, Xue Liang, Zhifeng Lei, Hailong Huang, Hui Wang, Xiongjun Liu, Ke An, Wei Wu & Zhaoping Lu (2019) Formation, structure and properties of biocompatible TiZrHfNbTa high-entropy alloys, Materials Research Letters, 7:6, 225-231, DOI: 10.1080/21663831.2019.1584592
3. Guo S, Ng C, Lu J, et al. Effect of valence electron concentration on stability of fcc or bcc phase in high entropy alloys. J Appl Phys. 109 (2011): 103505.
4. Stefan Schoenauer, Xiang Li, David J. Weber, et al. Harnessing elastic anisotropy to achieve low-modulus refractory high-entropy alloys for biomedical applications. Materials & Design 215 (2022) 110468.
5. Li X., Wang X., Zhang W., et al. Fabrication and characterization of porous TiZrHfNbTa alloy for biomedical applications using electron beam melting process. Mater. Lett. 289 (2019): 125-485.
6. Niinomi M. Mechanical properties of biomedical titanium alloys. Mater Sci Eng A. 243 (1998): 231-236.
7. Senkov ON, Scott JM, Senkova SV, et al. Microstructure and room temperature properties of a high-entropy TaNbHfZrTi alloy. J Alloy Compd. 509 (2011): 6043-6048.
8. Ikehata H., Nagasako N., Furuta T., et al. First-principles calculations for understanding high ductility and low modulus of TiNbTaZrHf high-entropy alloys. Scripta Mater. 135 (2017): 88-91.
9. Yuan Y., Wu Y., Tang X., et al. Rare-earth high-entropy alloys with giant magnetocaloric effect. Acta Mater. 155 (2018): 481-489.
10. Wang Y, Liaw PK, Pender M, et al. Microstructure and room temperature properties of a high-entropy TaNbHfZrTi alloy. Scripta Mater. 64 (2011): 957-960.
11. Guo S, Hu Q, Ng C, et al. More than entropy in high-entropy alloys: Forming solid solutions or amorphous phase. Intermetallics 31 (2012): 96-103.
12. Song Y., Xu W., Yang R., et al. Theoretical study of the mechanical properties of the Zr-Hf-Ti system and its alloys of β-type bio-titanium alloys. Mater Sci Eng A. 799 (2020): 115-257.
13. Liu CT. Physical metallurgy and mechanical properties of ductile ordered intermetallic alloys. Mater Chem Phys. 42 (1995): 77-86.
14. Labusch R. A statistical theory of solid solution hardening. Phys Status Solidi B. 41 (1970): 659-669.